

Behavior of C45 steel Subjected to Different High Pressure Torsion (HPT) Procedures

Mike Haddad

Institute of Micro and Nanomaterials
University of Ulm, Ulm
Germany

Yulia Ivanisenko

Institute of Nanotechnology
Karlsruhe Institute of Technology
Karlsruhe, Germany.

Hans-Jörg Fecht

Institute of Micro and Nanomaterials
University of Ulm, Ulm
Germany

Abstract

Steel, as an indispensable material in modern engineering and structural applications, continues to be highly relevant in the field of nanocrystalline materials. Devising innovative methods in addition to understanding the deformation physics of those materials are of great importance in modern research fields to enhance the superior properties of such materials. In this study, commercially available C45 steel (Fe, 0.42-0.5w% C, 0.5-0.8w% Mn) was processed with different high pressure torsion procedures leading to ultrafine/nano-scale grain size and improved mechanical properties. This study summarizes the mechanical properties, deformation behavior, and microstructure development of nanocrystalline C45 steel through in-situ tensile test measurements performed within the scanning electron microscope and supplemented by transmission electron microscopy analysis. It also outlines the characteristics of the warm high pressure torsion technique (WHPT) which improved the mechanical properties of the commercial C45 steel significantly and made it comparable with high strength high alloyed steels.

1. Introduction

The unique properties of nanostructured materials are of great importance for various advanced applications [1], and one of the materials that plays a fundamental and essential role in structural applications is the iron-carbon system[1, 2].

In the last decade, there was increasing interest in bulk nanocrystalline materials and specifically in those processed by the severe plastic deformation (SPD) methods such as high pressure torsion (HPT) and equal channel angular pressing (ECAP) which have been successfully implemented as novel processing techniques for producing nano and sub-microcrystalline metallic materials [3, 4].

By applying the SPD methods, grain refinement as well as phase transformations take place during the processing[1] resulting in an ultrafine grain size and a unique and extraordinary physical, chemical, and mechanical properties such as high yield stress and high tensile strength, which are often strongly enhanced in comparison with the properties of their coarse grained counterparts [5, 6]. The yield strength and the tensile strength for the C45 steel samples processed by WHPT were in the order of 1390 MPa and 2174 MPa respectively.

2. Experimental Procedures

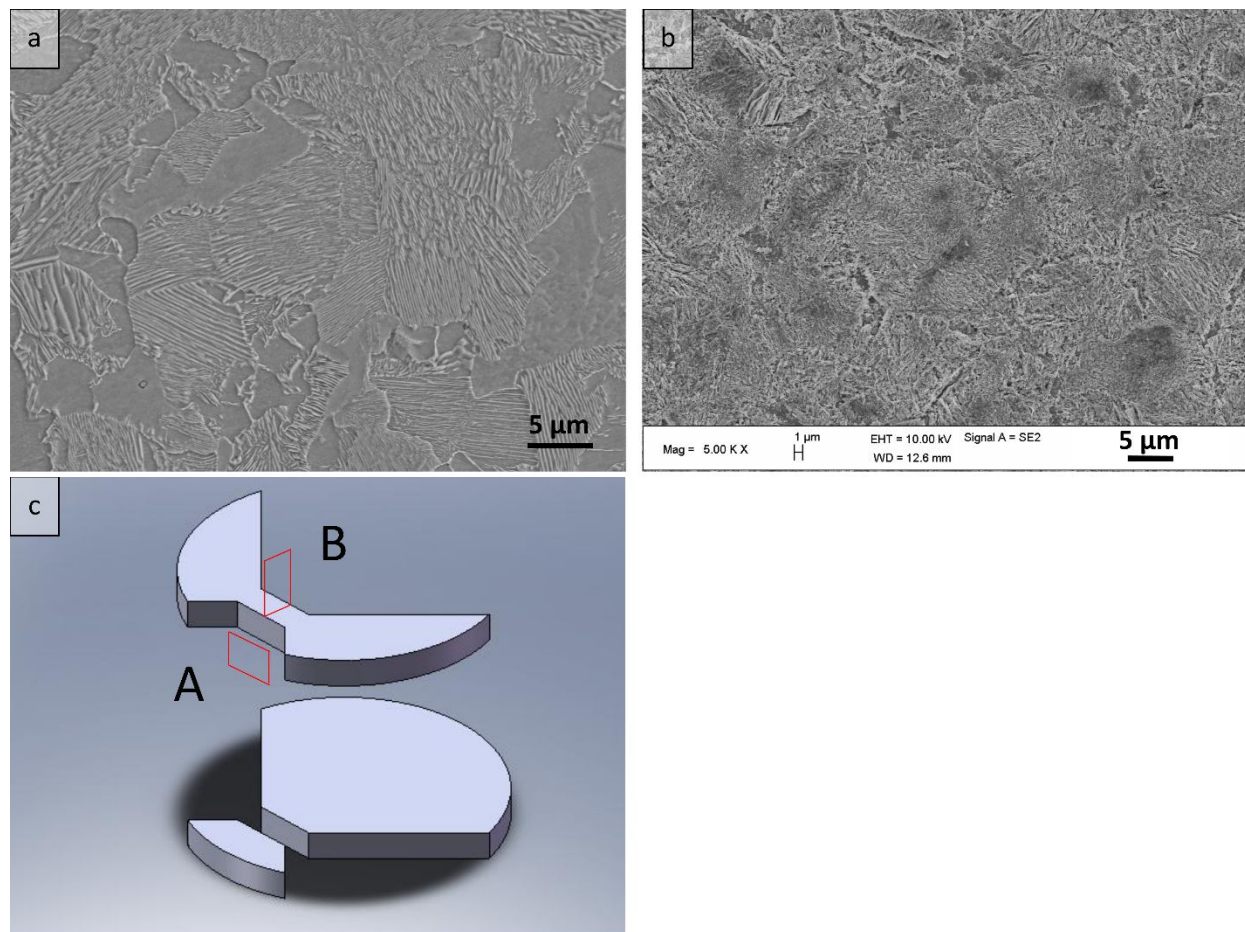


Figure 1: (a,b) SEM Images Showing the Microstructure of the C45 Steel: (a) as Delivered, (b) Patented. (c) Preparing Dog Bone Samples

Commercial medium carbon steel C45 (Fe - 0.44C, 0.65Mn, 0.18Si, 0.006S, 0.01P, all in wt%) with ferritic-pearlitic microstructure as shown in Figure (1a), was used. In order to obtain more homogeneous cementite distribution, special patenting treatment was performed. Upon that, C45 steel rods with 10mm diameter were heated up to 900°C for one hour then cooled down in 5 seconds to 500°C using molten lead bath and kept there for 30 minutes ending with upper bainite microstructure as depicted in Figure (1b).

Thereafter, C45 rods were cut into 0.7 mm thickness disks and processed by HPT under a pressure of 6 GPa for 3 and 5 rotations, using different processing temperatures: room temperature and 350°C.

Dog bone samples with 1.4 mm gauge length and 1 mm width, were cut from the HPT processed disks (Fig. 1c), then ground using silicon carbide grinding papers with different sizes (grit 1200, 2500, and 4000), and then polished using Colloidal silica suspension in order to remove surface defects as they are potential sources for stress concentration and subsequent failure. The same grinding and polishing procedures were used also for all SEM samples. Hardness measurements for the patented and the HPT processed samples were performed using Micromet 5103 Vickers microhardness tester (Buehler GmbH).

The *in-situ* tensile tests were performed under constant strain rate of $1.4 \times 10^{-4} \text{ s}^{-1}$ using MicroDAC tensile test stage (Kammrath and Weiss GmbH) which was installed inside a LEO 1550 high resolution field emission scanning electron microscope (FE-SEM).

Zeiss NVision 40 Ar and FEI Strata 400 focused ion beam (FIB) were used to extract and thin the transmission electron microscopy (TEM) samples. Afterward, 5 kV Ga⁺ beam was used to minimize FIB damage of the TEM lamella.

Philips CM30 TEM operated at 300kV was used for conventional TEM images while FEI Tecnai F20 TEM operating at 200 kV equipped with ASTAR system was used for the automated phase and crystal orientation mapping (ACOM) acquisition [7]. Orientation maps with an acquisition speed of 100 frames/second have been obtained.

3. Results and Discussion

3.1. Patented Samples Processed at Room Temperature

Hardness measurements performed after HPT for 5 rotations along the diameter of HPT-processed C45 samples showed a minimal enhancement slightly higher than the as-patented state value in the HPT disk center. The hardness increased rapidly while moving away from the center towards the edges and reached a value of more than 850 HV at a location 3 mm away from the center.

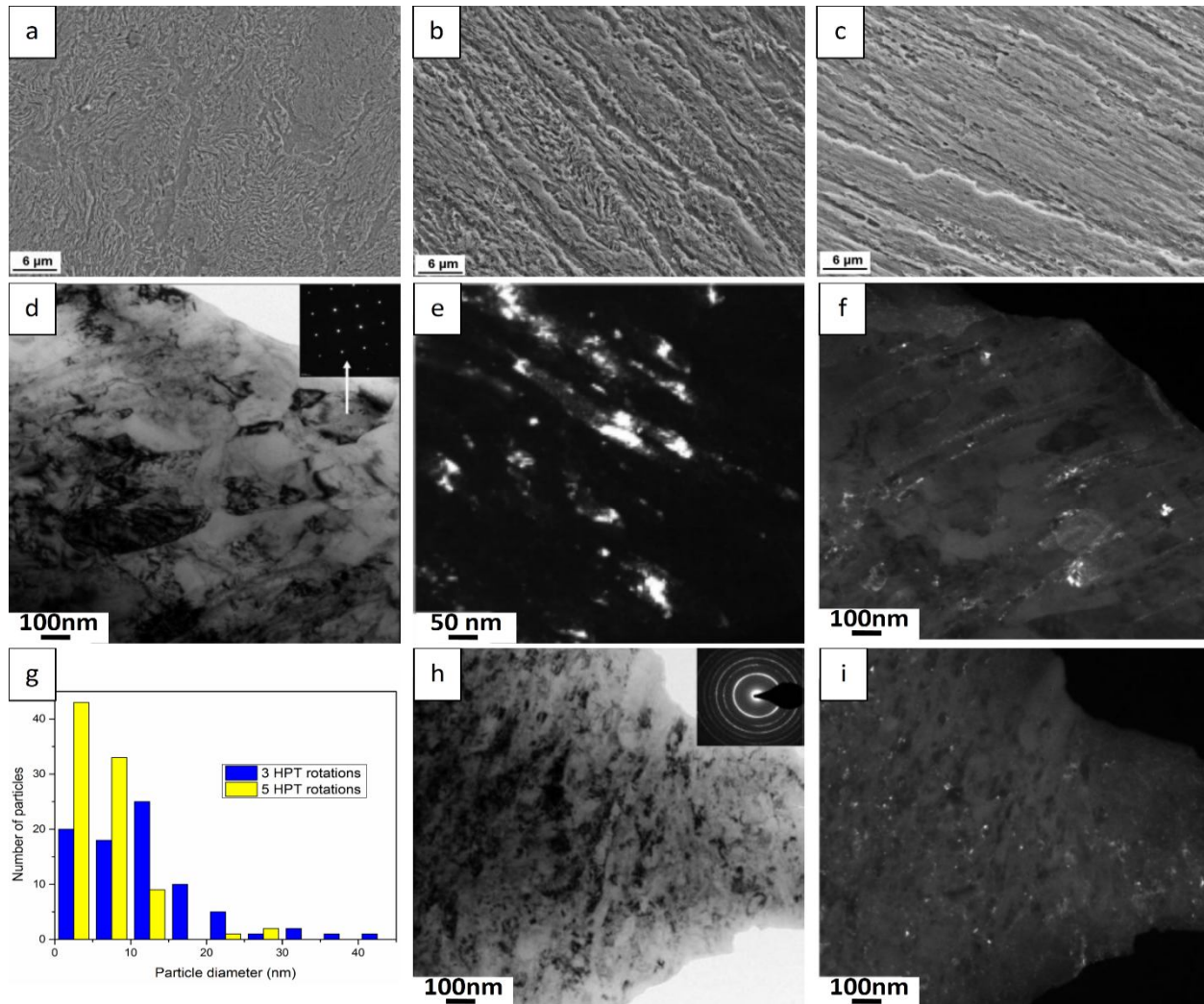


Figure 2: (a,b,c) SEM images taken at 0, 3 mm from the center after 3 HPT rotations, and 3 mm from the center after 5 HPT rotations, respectively. (d,e,f) TEM images showing the microstructure after 3 HPT rotations: (d) BF image showing the microstructure with SAED pattern; (e) DF image (created using a part of 110α and 200α rings) showing the elongated ferrite structure; (f) DF image (created using some of the cementite reflections within the 110α diffraction ring) showing equiaxed fragmented cementite particles. (g) Size distribution of the remaining cementite particles after 3 and 5 HPT rotations. (h,i) TEM images showing the microstructure after 5 HPT rotations: (h) BF image showing the homogeneous microstructure with SAED pattern; (i) DF image (created using some of the cementite reflections within the 110α ring) showing the homogeneously distributed equiaxed cementite particles. Images d to i are from [2].

In agreement with hardness measurements SEM observations showed almost intact bainitic microstructure in the center (Figure 2a), while at 3 mm away after 3 HPT rotations, strong cementite lamellae alignment in the shear direction was observed, also, some structureless areas could be resolved (Figure 2b) looking similar to the martensite obtained by quenching of carbon steels and to the White Etching Layer (WEL) on the surface of railways tracks [1, 8]. After 5 HPT rotations, separate cementite lamellae were not resolved any more, with the surface being covered by large smooth areas elongated in shear direction as depicted in Figure (2c).

Ning et al. [2] used the TEM to study the microstructure of the HPT processed samples on an area 3 mm away from the center. Their investigations after 3 HPT rotations revealed inhomogeneous microstructure when areas with almost equiaxed ferrite grains with dimensions of 150-400 nm (Figure 2d) can be seen together with areas with elongated grains (20-60 nm wide and 50-150 nm long), separated by high angle grain boundaries and dense dislocation walls (Figure 2e). In fact such boundaries are very similar to the lamellar-type boundaries in the banded-structures observed in heavily deformed metals [1]. Moreover, the cementite lamellas were broken and fragmented mainly into fine equiaxed particles with a notable alignment along the shear direction as shown in Figure (2f), which is comparable to the alignment of the cementite fragments along the wire axis in cold drawn pearlitic steel [9, 10, 11, 12]. The size of the cementite particles shows a wide distribution with grains of more than 40 nm as depicted in Figure (2g).

On the other hand, investigations of the sample microstructure after 5 HPT rotations revealed homogeneous equiaxed ferritic structure with estimated mean grain size in the order of 10 nm, while the SAED patterns depicted in Figure (2h) confirms that the structure is polycrystalline with nanoscaled crystallite sizes and high angle grain boundaries [2]. Furthermore, Figure (2i) shows that the cementite phase consists of very fine equiaxed particles distributed homogeneously in the structure without any recognized alignment as in the previous case. The size of the cementite particles shows more homogeneous and narrower distribution with finer grains as depicted in Figure (2g).

In addition to the fragmentation, dissolution process is taking place at a very beginning stage, as Sauvage et al. [13] used the Atom-probe tomography (APT) to study the pearlitic steel after HPT and found that 40% of the cementite dissolution took place at an early stage during HPT processing. In particular, the APT analysis affirms the formation of an off-stoichiometry cementite with carbon concentration gradient along the ferrite/cementite interfaces starting from the early stages of the HPT processing. As soon as the binding energy of carbon atoms in cementite lattice (0.4-0.42 eV), is less than that for dislocations with interstitials (0.5-1.0 eV), carbon atoms in the cementite near the interphase boundaries can jump to the dislocations in the ferrite, then some of them diffuse along the core of dislocations collected at the interfaces causing cementite decomposition and dissolution [1, 2, 9, 10, 14, 15, 16, 17]. Due to this decomposition during the HPT processing, the amount of cementite decreases effectively till it is almost fully decomposes and only few nanoclusters remain [1, 9, 18, 19, 20].

Tensile tests were carried out and the stress-strain diagram of the RT HPT processed samples were obtained and plotted in Figure 3a. Also, the stress-strain diagram of the as patented sample was plotted for comparison purposes. Despite the high strength of the RT HPT processed samples (around 2400 MPa), which is attributed to the finer grain size, they show very brittle behavior as the failure occurs immediately after the plastic flow onset. This brittle behavior is comparable with most bulk nanostructured materials as they also suffer from relatively low ductility [21, 22] due to the small grain size and the saturated dislocations density. Nano-sized grains will not have enough space for the dislocations to accumulate inside them [23] while the dislocations accumulation becomes difficult within the dislocations saturated samples [24]. Hence, such samples will suffer from limited strain hardening ability and therefore, severely reduce ductility [24].

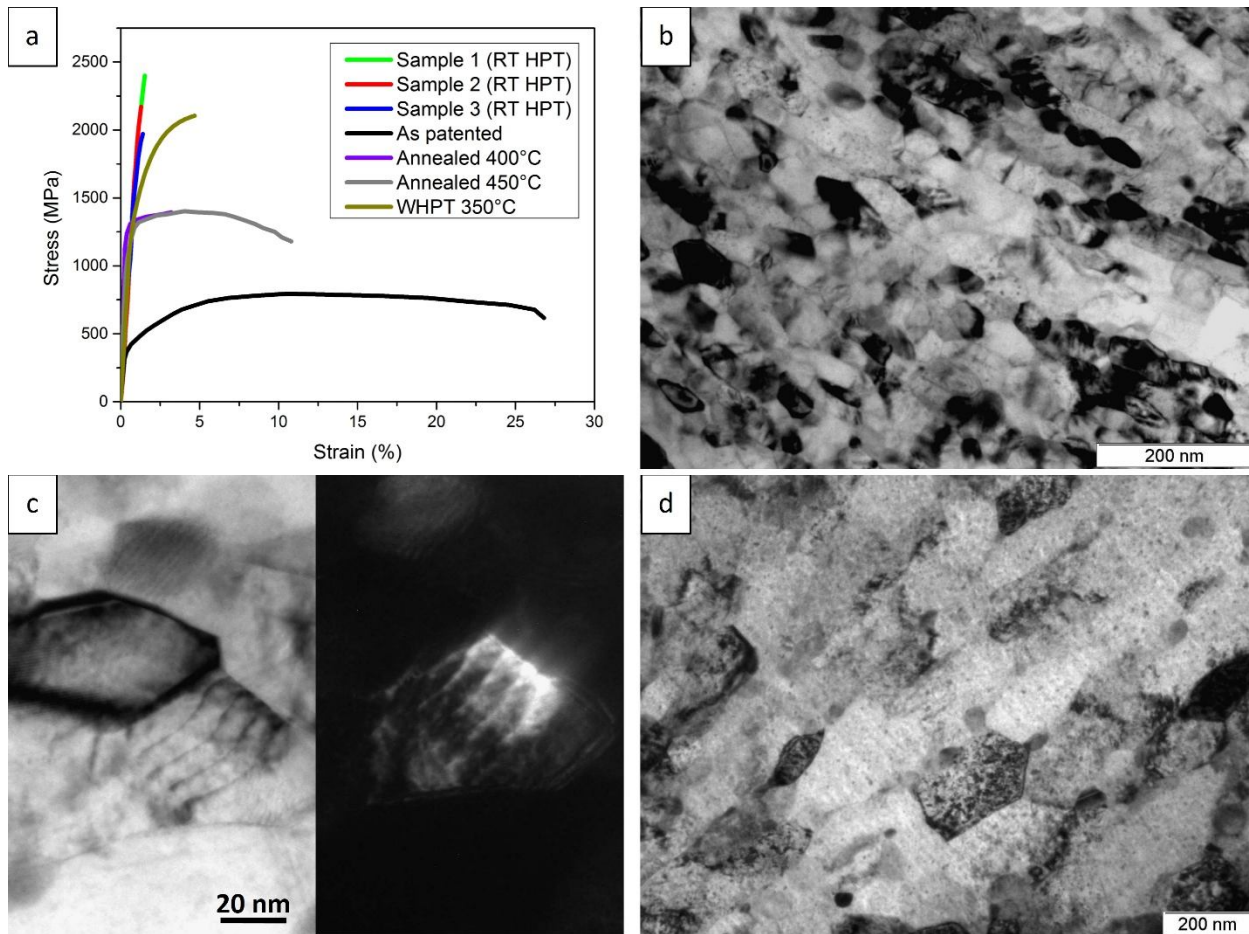


Figure 3: (a) stress-strain diagrams for as delivered and processed C45 samples. (b) TEM image showing the microstructure of the 400°C annealed sample. (c) BF and DF TEM images showing arrangements of dislocations. (d) TEM image showing the microstructure of the 450°C annealed sample. (For interpretation of the references to color in this figure legend, the reader is referred to the web version of this article.)

3.2. Annealing of the RT HPT Processed Samples

Annealing treatments at 400°C and 450°C for two hours were carried out to improve the low ductility of the RT HPT processed samples.

As depicted in Figure 3b, TEM investigations on the sample annealed at 400°C showed a microstructure consisting of a mixture of elongated and equiaxed grains. The grain size had not notably changed after annealing (63 nm in the shear direction and 26 nm in the radial direction), with more distinct grain boundaries and some grains containing high density of dislocations as shown in Figure 3c.

As soon as the mean grain size practically had not changed, but grain boundaries became narrower after annealing, it was concluded that continuous recrystallization, which is typical for severely deformed ferritic steels [25, 26, 27] has taken place.

The samples annealed at 450°C showed also a microstructure consisting of equiaxed and elongated grains as shown in the TEM image of Figure 3d, but this time, some grain growth took place as the mean grain size was 213 nm in the shear direction and 130 nm in the radial direction. The tensile curves of the annealed samples depicted in Figure 3a show UTS of 1397.5 MPa, yield strength of 1277.5 MPa, total elongation of 3%, and Vickers hardness of 655 for the 400°C annealed sample compared to 1384.4 MPa of UTS, 1071.5 MPa of yield strength, 556 HV for Vickers hardness, and a big elongation improvement in the order 11% for the 450°C annealed sample.

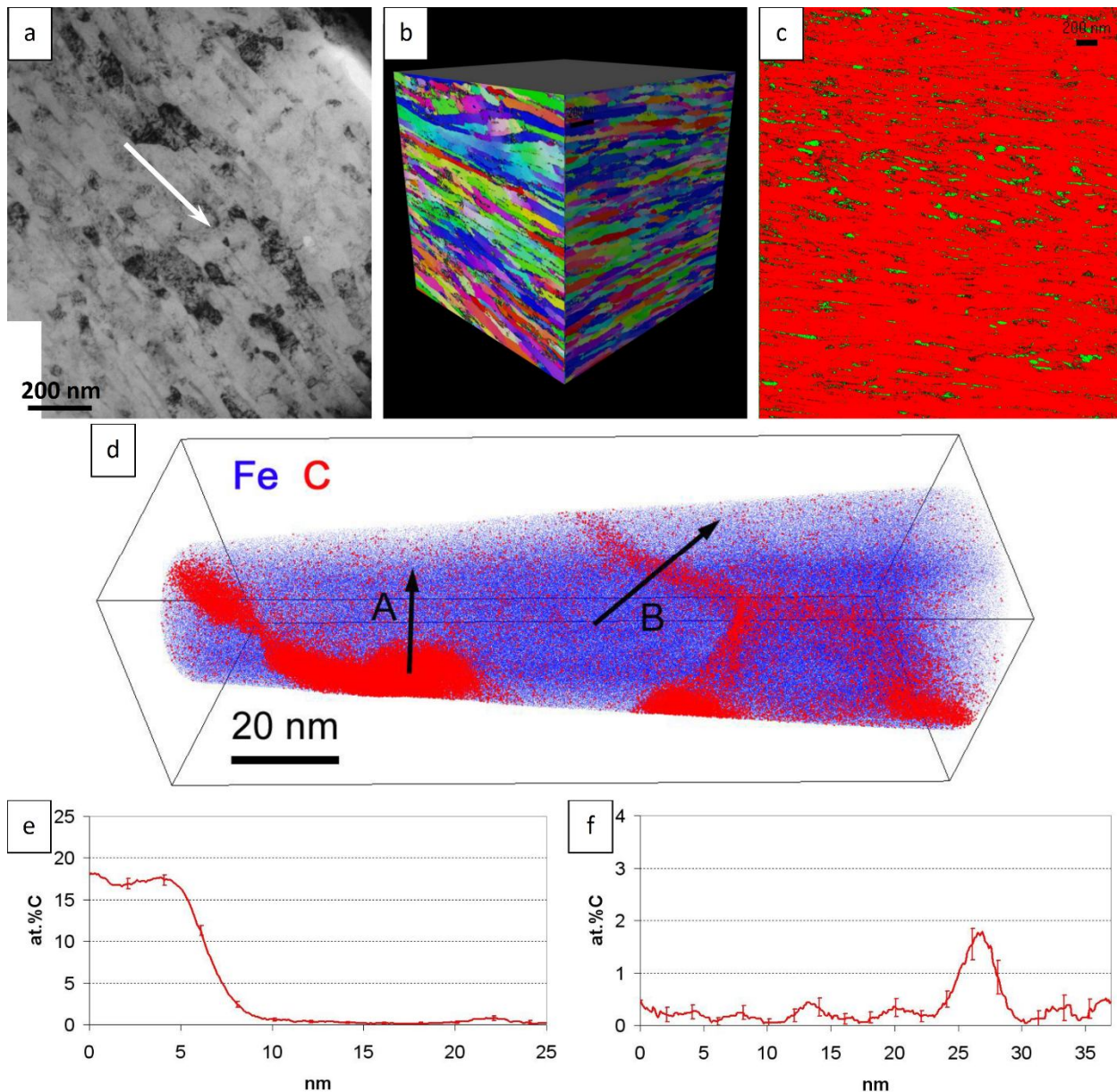


Figure 4: (a) TEM image showing the microstructure after WHPT and the arrow indicates shear direction. (b) Orientation maps created in radial and tangential directions [28]. (c) Corresponding 2-phases image, red (dark) color indicates ferrite while green (light) color indicates cementite [28]. (d) APT 3D reconstructed volume showing the heterogeneous distribution of carbon atoms (dark color). (e) Carbon concentration profile across a carbide/matrix interface (direction labeled A on the image (d)), sampling volume thickness 2 nm). (f) Carbon concentration profile across a segregation along a boundary (direction labeled B on the image (d)), sampling volume thickness 2 nm). Note: Images (d) to (f) are from [29].

3.3. Patented C45 Steel Processed by Warm HPT (WHPT)

Samples were HPT processed using the same previous procedure except that after mounting the sample, the HPT anvils were heated up to 350°C and this temperature was maintained with accuracy of $\pm 5^\circ\text{C}$ using induction heater during the HPT processing.

TEM and ACOM images in Figures(4a) and (4b) show a microstructure consisting of equiaxed and elongated (in shear direction) ferritic lamellas in nanoscale size. By applying the secant method to the ACOM image, the mean ferrite grain size was estimated to be 42 nm.

Figure (4c) shows irregularly shaped and strongly deformed cementite particles in the form of small islands homogeneously distributed in the ferrite matrix, mostly in between ferritic lamellae. They are resulting from fracture and fragmentation of the initial cementite lamellae during WHPT deformation. The cementite particles are located mostly at grain boundaries but some are also in the grain interior.

From the ACOM 2-phase image of Figure (4c), the area fraction of cementite was estimated to be 6.2% which is slightly lower than the equilibrium volume fraction of 7.8 vol.% according to the phase diagram. Considering that on one hand, ACOM missed the smallest particles, and on the other hand, we only see a projection of the cementite grains in the ferrite matrix, the high volume fraction of detected carbide suggests that cementite dissolution during WHPT was limited which is very different as compared to RT HPT processed C45 samples as well as to pearlitic steel processed by room temperature HPT[1, 2, 18, 13].

As studied by Sauvage et al [29] by means of the atom probe tomography (APT) carbon atoms are well partitioned in the patented C45 steel before HPT, most of them reside in Fe₃C carbides while a very small amount, typically less than 0.1%, is in solid solution in the bcc ferrite matrix. But after HPT, the carbon distribution has changed. The APT 3D reconstructed volume depicted in Figure (4d) shows both nanoscaled and elongated carbides (about 20 nm in length) exhibited together with some diffuse segregation along some boundaries. The composition profile computed across the carbide/matrix interface (Figure 4e) indicates that these carbides are partly dissolved and the carbon concentration is well below 25 at% as expected for stoichiometric cementite (Fe₃C carbide), it is only in a range of 15-20 at%, however, the crystal structure of these carbides is similar to that of Fe₃C as they are detected well by ACOM. Following this partial decomposition, carbon atoms released in the matrix do segregate along defects like boundaries where the local concentration is up to 2 at% (see the concentration profile Figure (4f)).

Table 1. Mechanical Properties of Various High Strength Steels and SPD Processed Steels

Material and processing	UTS, MPa	Elongation, %	Reference
C45	bainite	800	≥10
	WHPT	2150	3.7
Mart 1250/1520		1500	4 - 6
Nb-micro-alloyed	as-quenched	1750	7
AHSS	tempered	1500	13
Rail steel R260, ECAP		1540	-
Alloyed ferritic steel, HPT		1850	2.5
Alloyed austenitic steel, HPT		1850	1.5

As depicted in Figure (3a), the in situ tensile test of the WHPT processed samples ends up with a total elongation of 4.5% (plastic elongation of 3.7%), a yield strength of 1390 MPa and a UTS of 2174 MPa which are greater than these of some grades of advanced high strength steels (AHSS) and even martensitic steels as shown in Table 1. Furthermore, it is not surprising that the UTS of this sample is comparable with the RT HPT processed sample but with higher total strain as it has larger grains which provide more space within the grains for significant numbers of dislocations to intersect with each other and, consequently, accumulate during deformation [24]. Moreover, in comparison with the RT HPT processed sample, the WHPT processed sample had limited cementite dissolution as the fraction of cementite detected within the sample was high and it is well known that HPT processed samples which contain very fine cementite particles dispersed in UFG ferritic matrix will yield higher tensile ductility without losing the high strength[34, 35], And the grain boundary contribution to the yield strength was calculated in [28] and found to be 1375 MPa.

In agreement with the tensile curve, in-situ SEM observations (Figure 5a) affirm that the sample was deformed homogeneously with no traces of neck formation until fracture which is comparable with some grades of AHSS as they may break with minimal necking [36], and in other cases, it is difficult to visually identify the instability point [37]. Furthermore, facilitated plastic flow was recognized near all surface defects which visualized by shear bands formation as shown in Figure (5b), while the first indications of surface flow appeared at a stress level of 1480 MPa and 2.1% of total elongation.

With increasing the applied stress level, two cracks appeared at an angle of 35° , as depicted in Figure (5c), subsequently one of them propagated changing its direction to 90° to the tensile axis causing a slant through the thickness fracture as shown in Figure 5d.

The fracture surface is covered with very fine equiaxed dimples (Figure 5e) which indicates that the failure occurred by microvoid coalescence [38]. By increasing the strain, microvoids grow, coalesce, and eventually form a continuous fracture surface. The equiaxed shape of dimples indicates an uniaxial tensile overload failure as they form under conditions of uniform plastic flow in the direction of applied tensile stress [38]. Thus, the fracture has ductile character as the dimples indicate a tough fracture, and the failure occurred due to stress concentration at the surface flaw rather than the lack of ductility.

4. Conclusions

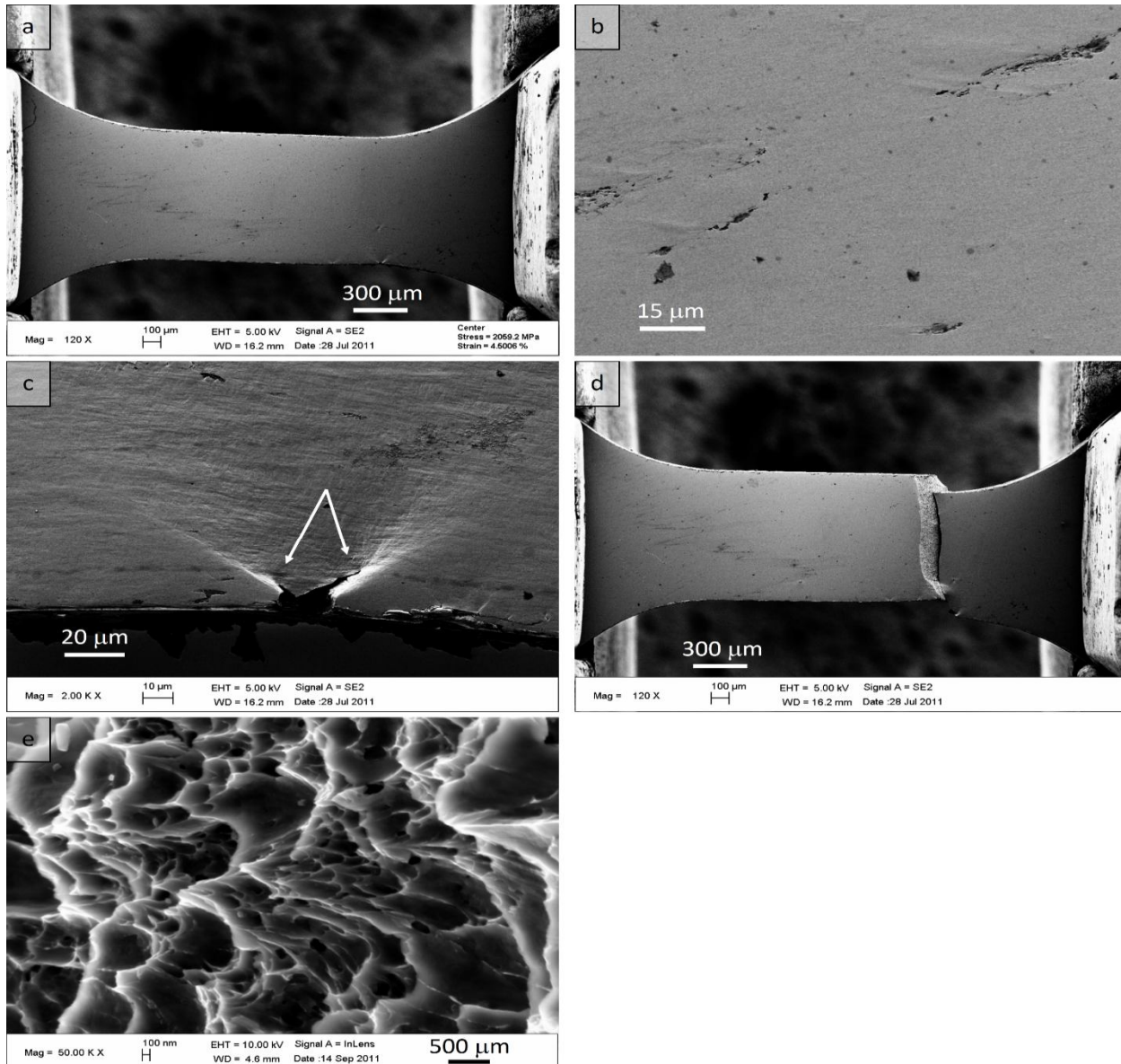


Figure 5: SEM images during in situ tensile test: (a) immediately before fracture. (b) Shear bands near surface defects. (c) Development of two cracks spreading at an angle of 35° to the sample edge (shown with arrows). (d) The sample after failure showing a slant fracture surface. (e) dimples covering the fracture surface.

- Room temperature HPT was efficient in grain refinement but did not provide flaw-free samples and showed very limited ductility due to macro and micro-cracks formation in addition to high level of macrostresses due to inhomogeneous strain distribution during HPT.
- Annealing the room temperature HPT processed samples at a temperature of 400°C for 2 hours caused continuous recrystallization with no grain size changes. After such annealing the ductility was notably improved, but the strength was reduced.
- WHPT presents a promising processing method for carbon steels to achieve enhanced mechanical properties. Outstanding combination of strength and ductility was obtained (1390 MPa of yield strength, 2100 MPa of UTS, and 3.7% of uniform plastic elongation). However, the full potential of this treatment has not been realized yet. Despite their strong refinement, the majority of cementite particles were located at ferrite grain boundaries, so their contribution to the strength and strain hardening capacity was only minor. Further attempts should be run to obtain a better intragranular distribution of cementite particles.

Acknowledgment

The authors would like to gratefully acknowledge U. Hörmann for doing a portion of the TEM investigations and the Deutsche Forschungs Gemeinschaft(projectFE313/13-1,IV98/2-1)for their generous financial support.

References

- [1] Y. Ivanisenko, W. Lojkowski, R. Valiev and H.-J. Fecht, *Acta Materialia*, vol. 51, pp. 5555--5570, 2003.
- [2] J. Ning, Y. Ivanisenko, D. Wang, M. Murashkin and H. Fecht, *Materials Science Forum*, Vols. 667-669, pp. 199-204, 2011.
- [3] Y. Ivanisenko, R. Wunderlich, R. Valiev and H.-J. Fecht, *Scripta Materialia*, vol. 49, pp. 947--952, 2003.
- [4] A. Belyakov, R. Kaibyshev, Y. Kimura and K. Tsuzaki, *Materials Science Forum*, Vols. 638 - 642, pp. 1905-1910, 2010.
- [5] A. Azushima, R. Kopp, A. Korhonen, D. Yang, F. Micari, G. Lahoti, P. Groche, J. Yanagimoto, N. Tsuji, A. Rosochowski and A. Yanagida, *CIRP Annals - Manufacturing Technology*, vol. 57, pp. 716--735, 2008.
- [6] H. Gleiter, "Nanostructured materials: basic concepts and microstructure," *Acta Materialia*, vol. 48, pp. 1-29, 2000.
- [7] E. Rauch, J. Portillo, S. Nicolopoulos, D. Bultreys, S. Rouvimov and P. Moeck, *Zeitschrift für Kristallographie*, vol. 225, p. 103--109, 2010.
- [8] M. Djahanbakhsh, W. Lojkowski, G. Bürkle, G. Baumann, J. Ivanisenko, R. Valiev and H. J. Fecht, *Journal of Metastable and Nanocrystalline Materials*, Vols. 360-362, pp. 175-182, 2001.
- [9] J. Languillaume, G. Kapelski and B. Baudelet, *Acta Materialia*, vol. 45, pp. 1201-1212, 1997.
- [10] X. Sauvage, W. Lefebvre, C. Genevois, S. Ohsaki and K. Hono, *Scripta Materialia*, vol. 60, pp. 1056-1061, 2009.
- [11] J. Embury and R. Fisher, *Acta Metallurgica*, Vols. 147-159, p. 14, 1966.
- [12] G. Langford, *Metallurgical Transactions A*, vol. 8A, pp. 861-875, 1977.
- [13] X. Sauvage and Y. Ivanisenko, *Journal of Material Science*, vol. 42, pp. 1615-1621, 2007.
- [14] V. N. Gridnev, V. V. Nemoshkalenko, Y. Meshkov, V. G. Gavriljuk, V. G. Prokopenko and O. N. Razumov, *Physica Status Solidi (A)*, vol. 31, pp. 201-210, 1975.
- [15] V. N. Gridnev, V. G. Gavriljuk, I. Y. Dekhtyar, Y. Y. Meshkov, P. S. Nizin and V. G. Prokopenko, *physica status solidi (a)*, vol. 14, no. 2, pp. 689-694, 1972.
- [16] V. Gavriljuk, *Materials Science and Engineering: A*, vol. 345, no. 1-2, pp. 81-89, 2003.
- [17] Y. Li, P. Choi, C. Borchers, S. Westerkamp, S. Goto, D. Raabe and R. Kirchheim, *Acta Materialia*, vol. 59, no. 10, pp. 3965-3977, 2011.
- [18] Y. Ivanisenko, I. MacLaren, X. Sauvage, R. Valiev and H.-J. Fecht, *Acta Materialia*, vol. 54, pp. 1659-1669, 2006.

- [19] W. Lojkowski, M. Djahanbakhsh, G. Buerkle, S. Gierlotka, W. Zielinski and H.-J. Fecht, *Materials Science and Engineering: A*, vol. 303, pp. 197-208, 2001.
- [20] A. Korznikov, Y. Ivanisenko, D. Laptionok, I. Safarov, V. Pilyugin and R. Valiev, *Nanostructured Materials*, vol. 4, pp. 159-167, 1994.
- [21] Y. Zhu and X. Liao, *Nature Materials*, vol. 3, pp. 351-352, 2004.
- [22] C. Koch, *Scripta Materialia*, vol. 49, no. 7, pp. 657-662, 2003.
- [23] Z. Budrovic, H. Van Swygenhoven, P. M. Derlet, S. Van Petegem and B. Schmitt, *Science*, vol. 304, pp. 273-276, 2004.
- [24] Y. Zhao, Y. Zhu and E. J. Lavernia, *Advanced Engineering Materials*, vol. 12, p. 769-778, 2010.
- [25] A. Belyakov, T. Sakai, H. Miura, R. Kaibyshev and K. Tsuzaki, *Acta Materialia*, vol. 50, pp. 1547-1557, 2002.
- [26] A. Belyakov, Y. Sakai, T. Hara, Y. Kimura and K. Tsuzaki, *Materials Science Forum*, Vols. 467 - 470, pp. 229-234, 2004.
- [27] A. Belyakov, Y. Kimura and K. Tsuzaki, *Materials Science Forum*, Vols. 503 - 504, pp. 323-328, 2006.
- [28] M. Haddad, Y. Ivanisenko, E. Courtois-Manara and H.-J. Fecht, *Materials Science and Engineering: A*, vol. 620, pp. 30-35, 2014.
- [29] X. Sauvage, A. Ganeev, Y. Ivanisenko, N. Enikeev, M. Murashkin and R. Valiev, *Advanced Engineering Materials*, vol. 14, p. 968-974, 2012.
- [30] R. Kuziak, R. Kawalla and S. Waengler, *Archives of Civil and Mechanical Engineering*, vol. 8, pp. 103-117, 2008.
- [31] N. Zhong, X. Wang, L. Wang and Y. Rong, *Materials Science and Engineering: A*, vol. 506, pp. 111-116, 2009.
- [32] F. Wetscher, R. Stock and R. Pippan, *Materials Science and Engineering: A*, Vols. 445-446, pp. 237-243, 2007.
- [33] A. Vorhauer, S. Kleber and R. Pippan, *Materials Science and Engineering: A*, Vols. 410-411, pp. 281-284, 2005.
- [34] J. Ning, E. Courtois-Manara, L. Kurmanaeva, A. Ganeev, R. Valiev, C. Kübel and Y. Ivanisenko, *Materials Science and Engineering: A*, vol. 581, pp. 8-15, 2013.
- [35] T. Lee, C. H. Park, D.-L. Lee and C. S. Lee, *Materials Science and Engineering: A*, vol. 528, pp. 6558-6564, 2011.
- [36] B. Yan, *Progress and challenges in forming AHSS*, Ohio State University, Columbus, OH, 2009.
- [37] A. Nasser, A. Yadav, P. Pathak and T. Altan, *Journal of Materials Processing Technology*, vol. 210, pp. 429-436, 2010.
- [38] ASM handbook, *Fractography*, Volume 12, 9th ed., 1992.